

AVO measurements for P-P and P-S data in the Blackfoot 3C-3D dataset

Vladan Simin, Gary F. Margrave, and Grace Y.C. Yang

ABSTRACT

We present a reconnaissance look at P-P and P-S amplitude variation with offset (AVO) effects for the Glauconite interval in the Blackfoot 3C-3D survey. Zoeppritz equations analysis from blocky models and raytrace synthetic seismograms built from three dipole sonics in the Blackfoot field predict discernible P-P (and possibly P-S) AVO effects associated with both the upper and lower porous sand channels. These effects are largely due to the anomalously low Poisson's ratio of these sands.

The Sensor processed subvolume was selected for analysis because of its smaller size and possibly higher signal band. The simple method of differencing offset limited migrated cubes to create maps of AVO anomalies. Three offset limited stacks formed from overlapping offset bins which together span the available offsets at the target time were formed for both vertical component and radial component data. The vertical component was processed for P-P reflections while the radial component was processed for P-S reflections. The six offset limited stacks were then run through a flow of time variant spectral whitening, fxy spatial prediction, and 3-D migration.

The six migrated volumes were then differenced (far-near for P-P and far-middle for P-S) and the difference volumes were inspected for AVO effects. Strong, obvious P-P AVO anomalies were found which indicate both the upper and lower channels. The top channel trend shows high lateral resolution and follows closely the trend of producing wells. The lower (Glauconite) channel is also imaged as a slightly more diffuse trend roughly 100-200 meters west of the producing oil wells. P-S AVO anomalies were also found in the channel interval with suggestive correlations but they are less interpretable due, in part, to our technique which is designed for P-P data.

INTRODUCTION

Shortly after the CREWES project acquired the Blackfoot broad-band dataset in the summer of 1995 (Stewart et al. 1996) we became aware that there was an interesting AVO (amplitude variation with offset) anomaly in the P-P data which seemed to correlate spatially with prospective Glauconite channel sands. Since AVO anomalies have been used successfully in sandstone exploration plays throughout the world (Ostrander 1984, Smith and Gidlow 1987, Ross and Beale, 1994), we felt that the anomaly was worth investigating. The acquisition of the Blackfoot 3C-3D (Stewart et al. 1996) over the established Blackfoot field presented us with a unique opportunity to assess the anomaly in 3D and compare it with good well control.

Figure 1 shows a basemap of the Blackfoot field and indicates the area covered by the 3C-3D survey. As explained in Simin et al. (1996) there are two alternative processed datasets presently available to us from Pulsonic Geophysical and Sensor Geophysical. Though this is a rich dataset with tremendous potential, it has only been available to us in a form suitable for this study since early October of this year. Therefore, we elected to conduct a "reconnaissance" look at P-P and P-S AVO effects in one of the datasets. By reconnaissance we mean that we have employed a simple technique using offset limited stacking to provide areal (time slice) views of potential

AVO anomalies. We have not had time to conduct detailed analyses or inversions with focused common reflection point gathers.

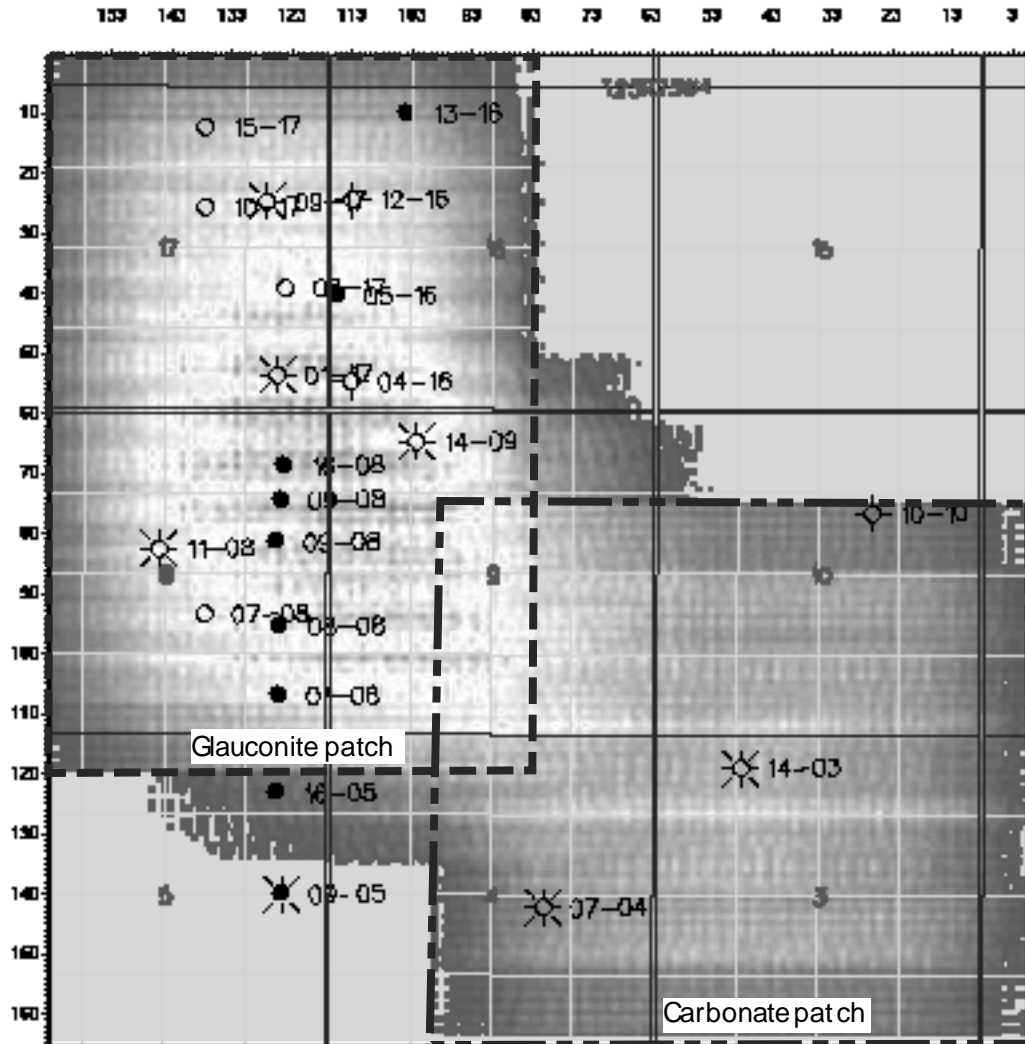


Fig. 1. The Blackfoot 3C-3D survey is shown consisting of a high fold Glaucanite patch and a lower fold carbonate patch. The Glaucanite patch was processed by Sensor Geophysical while the entire survey was processed by Pulsonic Geophysical.

The Sensor processed dataset was chosen for this investigation because it was smaller, focused on the Glaucanite patch, available first, and initially felt to be of higher quality. We now feel that the signal band of the Pulsonic data may be higher (see Schoepp and Margrave 1996, and Yang et al. 1996 for more discussion on both datasets) and intend to investigate that dataset in the near future.

METHOD

Our analysis begins with fully processed, binned, but unstacked data for both the vertical and radial components. The vertical component was processed for P-P reflections and the radial for P-S reflections. For each component, three overlapping offset bins were selected which spanned the range of offsets available at the reflection time of the channel. These bins, termed near, middle and far, were 0-900m, 500-1600m, and 1200-2100m for both P-P and P-S data. Our starting dataset had first

break and NMO stretch mutes applied so that there was no concern that the far offset information might be contaminated by refractions.

Three limited offset stacks were then formed for both P-P and P-S for a total of six stacked volumes. Each stacked volume was then processed in exactly the same manner as the original Sensor processing flow through 3D migration. This flow consisted of time variant spectral whitening (TVSW), f-x spatial prediction, and phase shift 3D migration.

The six migrated volumes were then used to form difference volumes which should provide a gross overview of the P-P and P-S AVO effects. At this time, we have only examined the far-near P-P difference dataset and the far-middle P-S dataset and these have only been studied in the vicinity of the Glauconite channel.

THEORETICAL EXPECTATIONS

Simplified theoretical predictions of the expected AVO behavior of reflectors in the target interval can be made by first blocking the relevant well logs into a few coarse lithologies and then raytracing P-P and P-S events off the relevant reflectors. (A Matlab utility called *zoepplot* is included in the current software release which made the plots shown here.) Figures 2, 3, and 4 show blocky versions of the Blackfoot 08-08, 12-16, and 9-17 logs. All three wells have dipole sonics and density logs and a Poisson's ratio log computed from v_p and v_s is also shown. Blackfoot 08-08 is a good producing oil well which encountered both upper and lower (Glauconite) channels, 12-16 also encountered channel but was shale plugged, and 9-17 is regional. Note that the top channel (glau_ch_top to glauc_1 on figure 3) and the Glauconite channel (glauc_ss_top to glauc_base) are characterized by a strong drop in Poisson's ratio. Blackfoot 12-16, though it encountered 50 meters of channel shows only a thin streak of low Poisson's ratio. Blackfoot 09-17, which encountered no channel, shows a thin highly anomalous Poisson's ratio drop associated with the Bantry Shale. This is felt to be a highly unlikely number and we consider it suspect; however, it was left unaltered for the analyses presented here.

Figures 5, 6, and 7 show computed Zoeppritz equations reflection coefficients (Aki and Richards, 1980) for each of the three blocky well models. Only reflections in the target zone are analyzed. In each figure, two graphs show the P-P reflections (A and B) and two show the P-S reflections (C and D). The reflection coefficients are plotted versus source-receiver offset in A and C and versus P-wave incidence angle in B and D. In each case, only the real part of the coefficient is shown though reflections beyond critical incidence angles will have a non-zero imaginary part which corresponds to a phase rotation. (Only the P-S Ostracod reflection in figure 7 reached a critical angle (about 58°).)

Comparing the P-P glauc_ch_top reflections in figures 5 and 6 shows that the sand filled channel should be distinguished from the shale filled channel by having a much stronger negative AVO effect. That is, both reflections are near -.05 at normal incidence but the sand filled channel nearly triples that value (-.15) by 2000m offset while the shale filled channel hardly changes. If viewing these on stacked data, we would expect that the channel would be indicated by a strengthened trough just below the Lower Mannville; however, an AVO analysis would be much more diagnostic. Comparing the corresponding P-S reflections is quite a different story but they still appear distinct. The sand channel and the shale channel are roughly reverse polarity versions of one another.

Another point of interest is the relative strength of the P-S reflection off of the Glaucosite channel (glauc_ss_top) versus the P-S reflection from the top channel (glauc_ch_top). From this, it might be expected that the lower (Glaucosite) channel will be more easily imaged on the P-S data than the upper channel; and this is observed to be the case (Yang et. al. 1996).

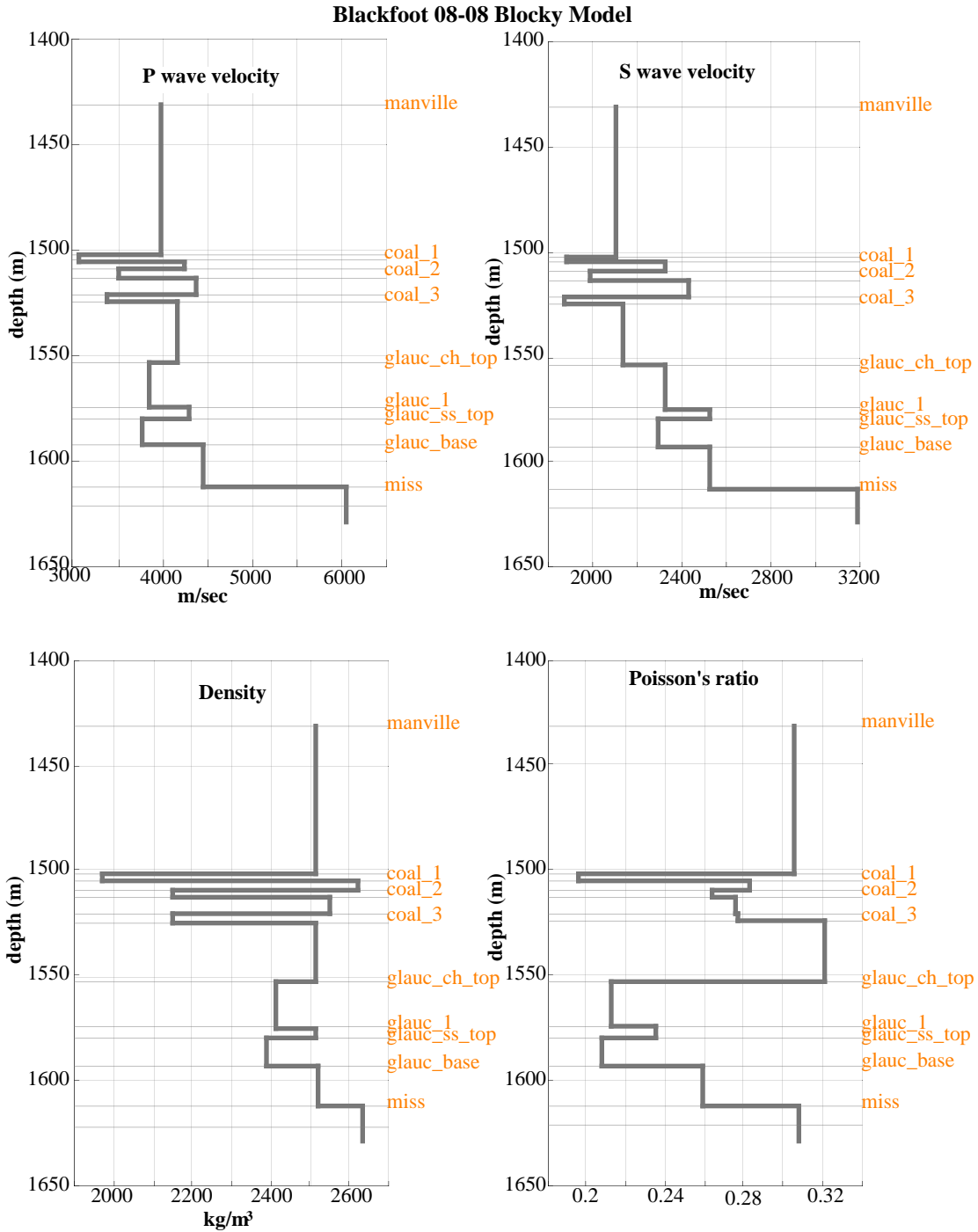


Fig. 2. Blocky versions of the Blackfoot 08-08 oil well. Note the strong Poisson's ratio drop at the channel.

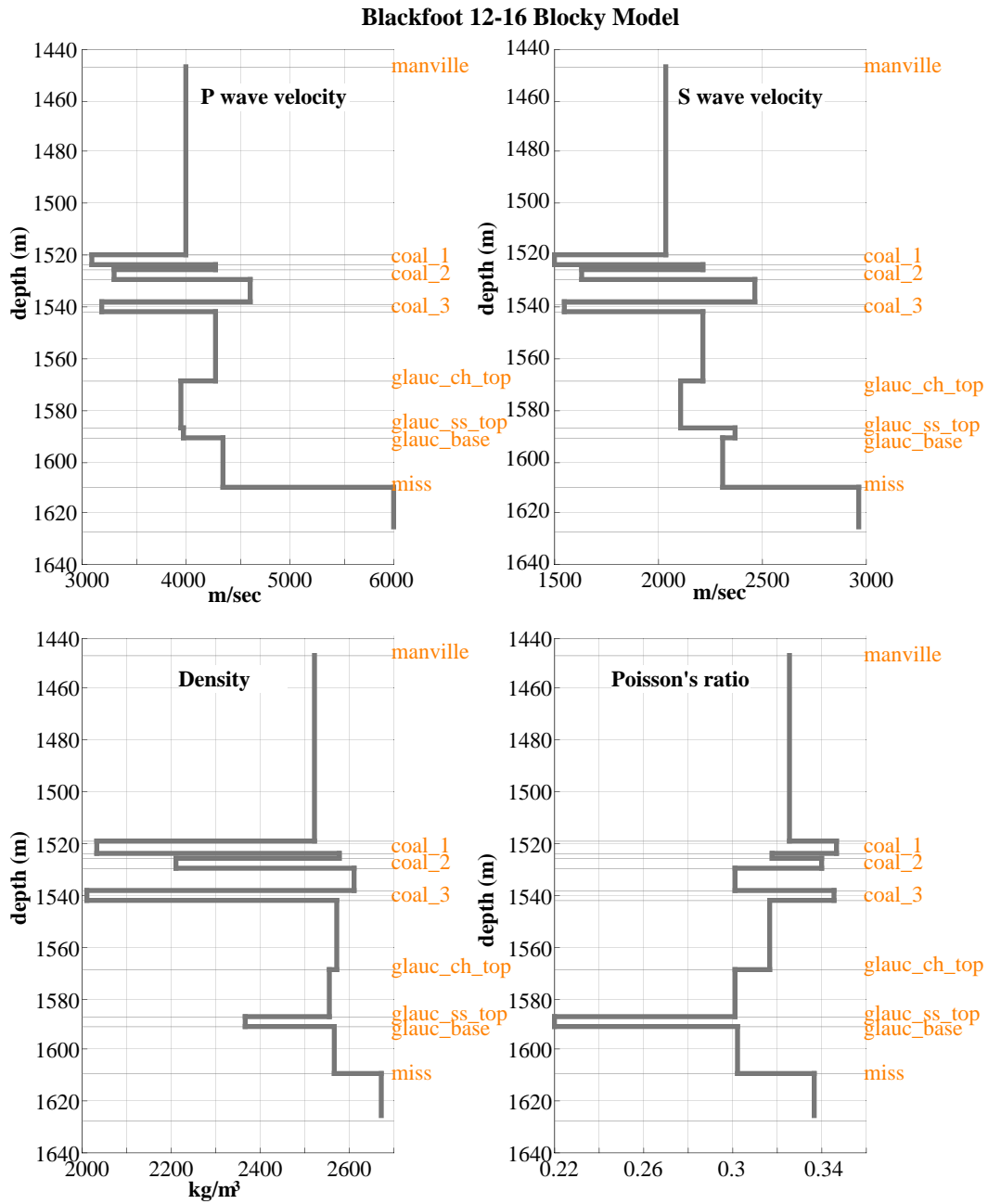


Fig. 3. Blocky versions of the Blackfoot 12-16 well. The well encountered shale filled channel. Compared with 08-08, there is little indication of the strong Poisson's ratio anomaly found there.

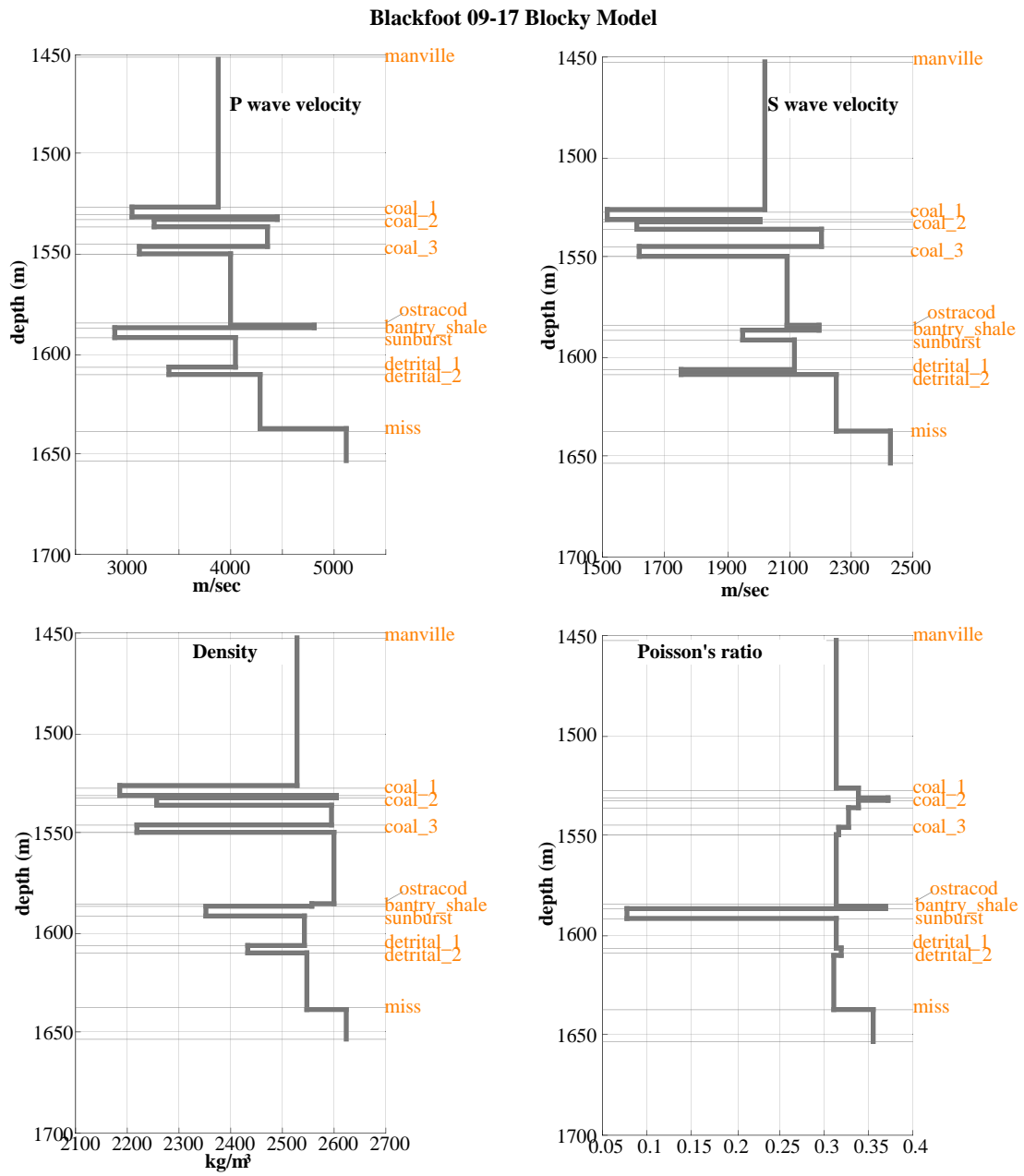


Fig. 4. Blocky versions of the Blackfoot 09-17 well. The Poisson's ratio anomaly at the Bantry Shale is considered unlikely.

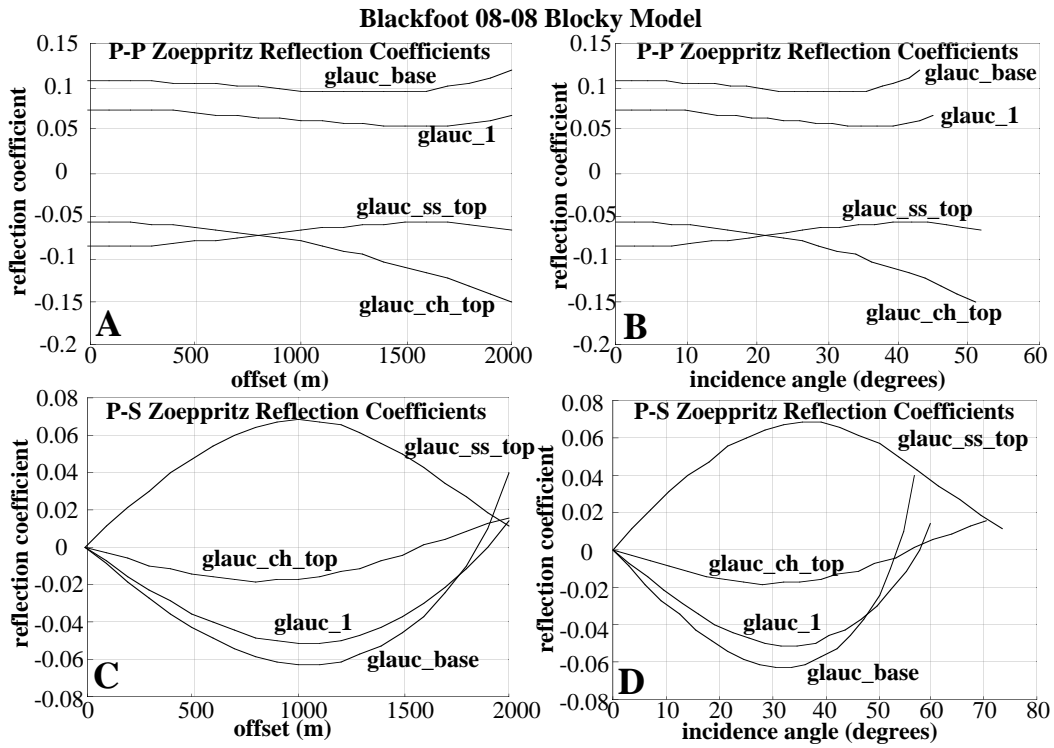


Fig. 5. Zoeppritz reflection coefficients computed by raytracing through the blocky model in figure 2.

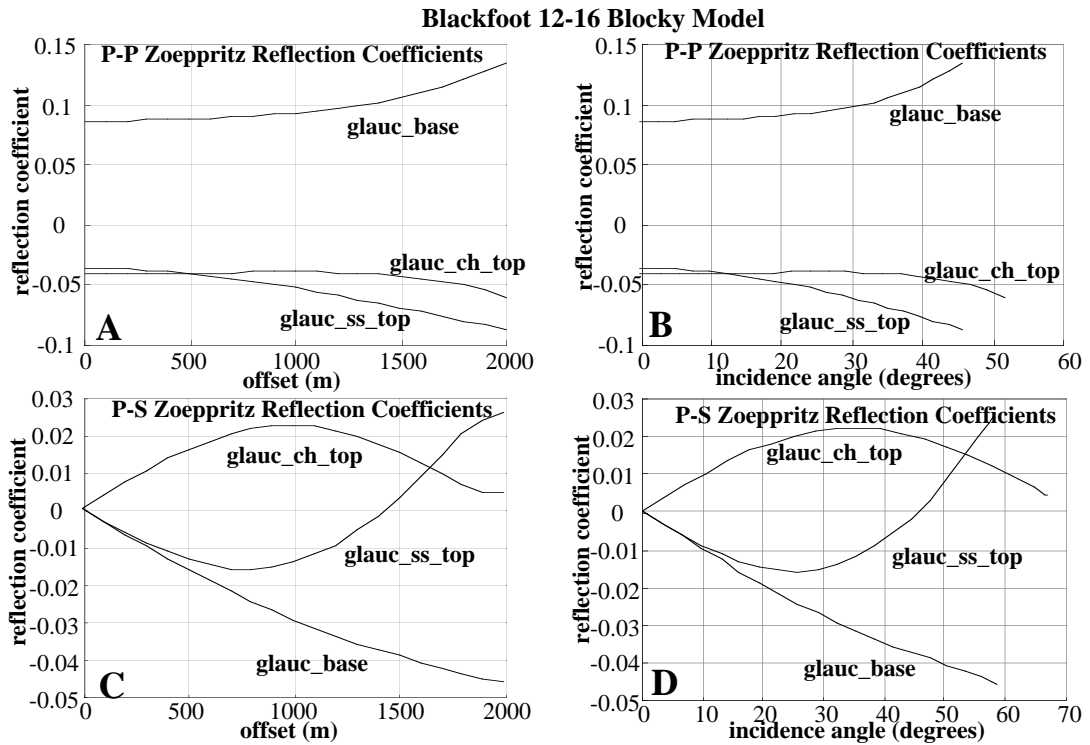


Fig. 6. Zoeppritz reflection coefficients computed by raytracing through the blocky model in figure 3.

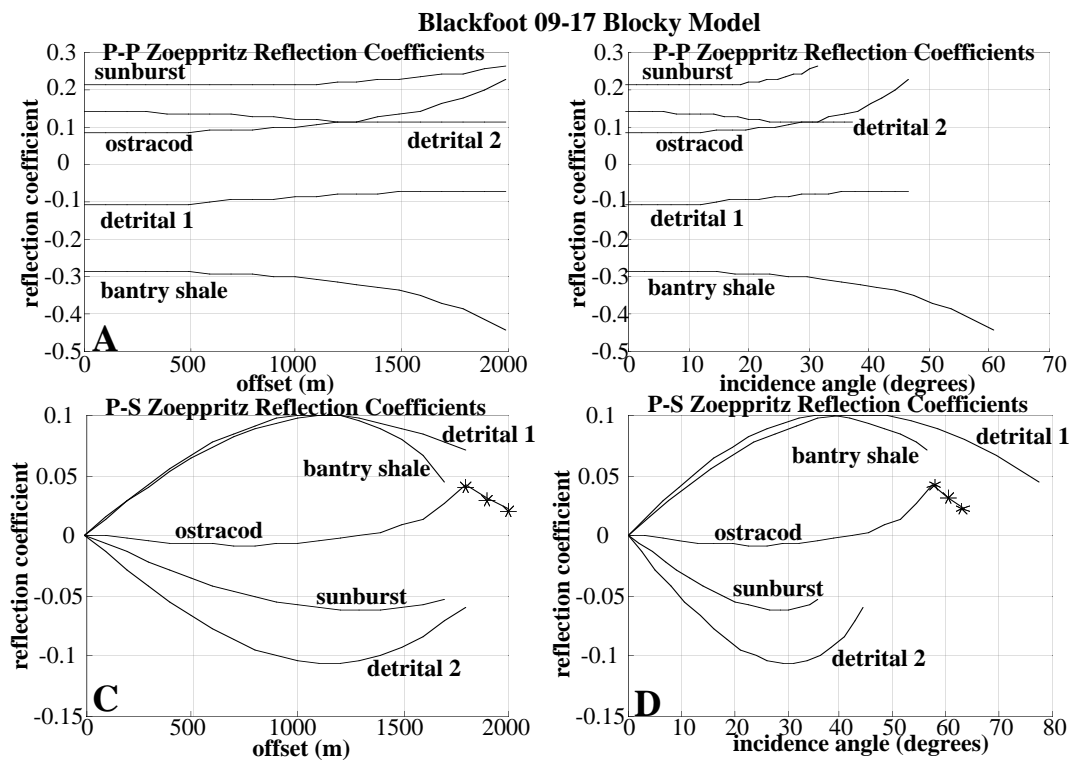


Fig. 7. Zoeppritz reflection coefficients computed by raytracing through the blocky model in figure 4. Points marked with an asterisk indicate complex reflection coefficients corresponding to post-critical reflections (only the real part is shown).

On 09-17, the Ostracod reflection should be stratigraphically near the channel reflections and can be seen to have a substantially different polarity and AVO. The detrital_1 reflection might also be confused with the channel top reflections but again has quite different AVO. However, a stack of the detrital might give a very similar result to a stack of the glauc_ch_top.

The results from the blocky models are intriguing but lack the realism derived from detailed seismogram computations. The construction of a block model imposes a bias with the choice of which intervals are significant and should be represented by a block. Figure 8 shows P-P and P-S synthetic seismograms computed from the Blackfoot 08-08 well using the SYNTH algorithm (Lawton and Howell, 1992, Margrave and Foltinek, 1995). (The time scales on the synthetics shown here have not been shifted to precisely match the real data.) The SYNTH algorithm produces only primaries with the Zoeppritz equations used for reflectivity calculations. As pointed out by Simmons and Backus (1994) this can be potentially misleading as the effect of interbed multiples and mode conversion can materially alter the theoretical seismogram. Additionally, the effects of NMO tuning and stretch are not included in these seismograms.

As is evident, there is considerable variation of P-P reflection strength with offset on a number of different reflections. Of interest here are the reflections above the top channel and above the lower channel (Glaucosite) which both show positive amplitudes which decrease with offset. Referring to figure 5A, the latter could possibly be interpreted as the glauc_base reflection while the former is not modeled. There is considerable character in the 08-08 log (not shown) between the bottom of the coals and the top of the channel and it is likely that we are seeing a composite (tuned) response of the top channel and the interval just above it.

The P-S synthetic seismogram varies much more strongly with offset as expected since the P-S reflection coefficient must vanish at normal incidence. It is not clear to us what, if any, of this behavior might be indicative of exploration targets.

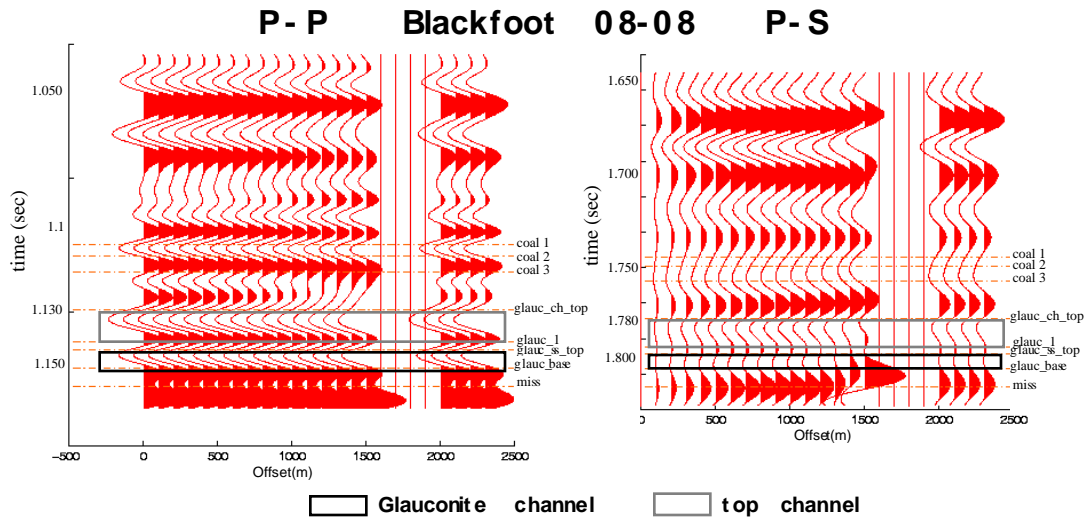


Fig. 8. Primaries only synthetic seismograms (computed with the SYNTH algorithm) are shown for the Blackfoot 08-08 well which is an oil well producing from the Glauconite channel.

Figures 9 and 10 show similar synthetics for the 12-16 well (shale plugged channel) and the 09-17 well (regional). Comparing them in detail with figure 8 is required to fully assess the theoretical expectations and we have not yet done that. Nevertheless, it seems that the P-P AVO decrease at the channel top is more pronounced on the 08-08 seismogram than on the other two. (Since there is no channel in 09-17, the comparison must be made to something at a similar stratigraphic level which would probably be the reflection just below the lower coal.)

Thus we might expect a negative AVO anomaly on the P-P data and make no predictions at this time for the P-S data.

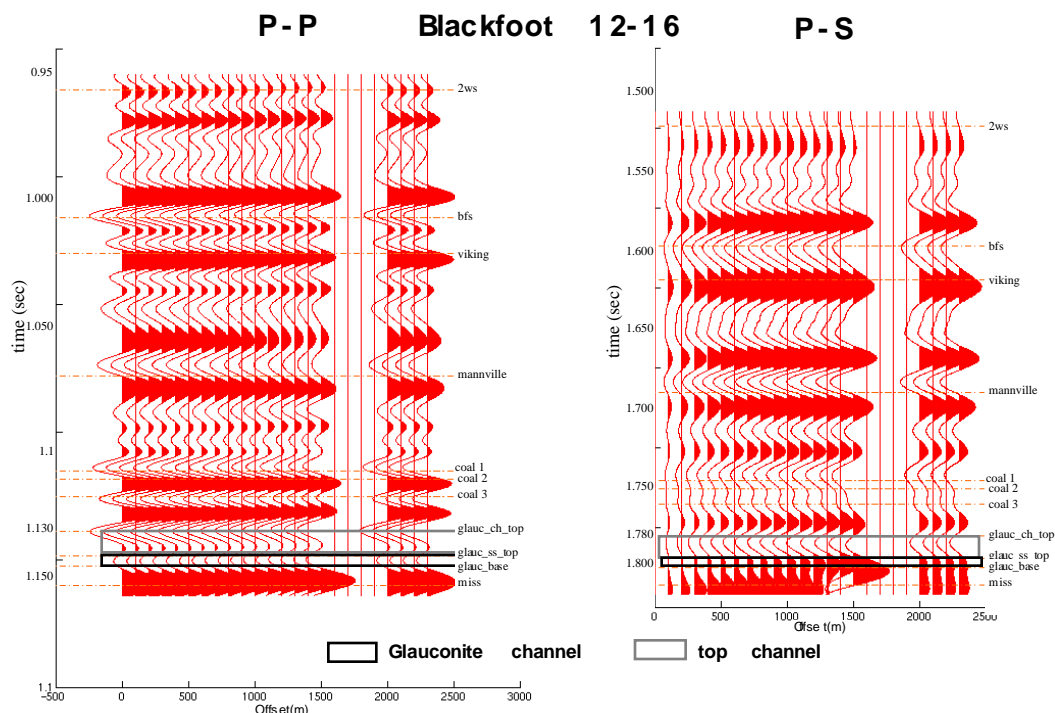


Fig. 9. Primaries only synthetic seismograms (computed with the SYNTH algorithm) are shown for the Blackfoot 12-16 well which encountered a shale plugged channel.

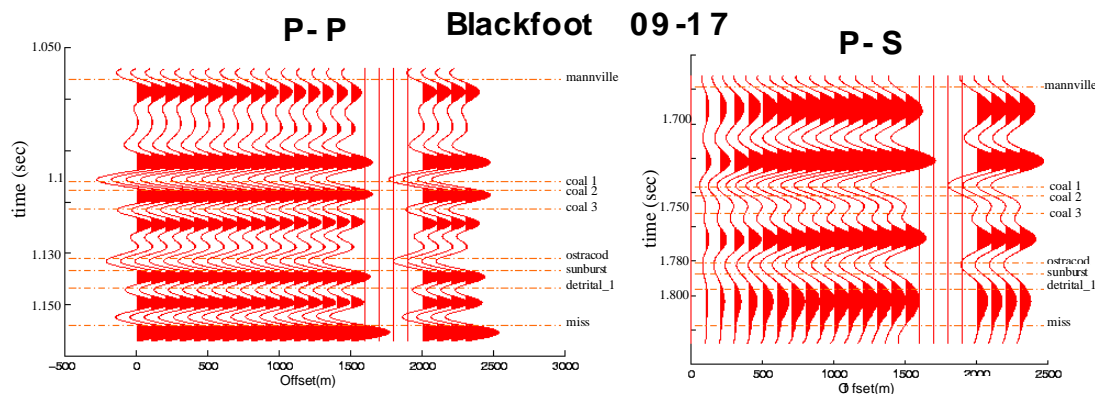


Fig. 10. Primaries only synthetic seismograms (computed with the SYNTH algorithm) are shown for the Blackfoot 09-17 well which encountered a regional environment (no channel).

RESULTS

The comparison of the limited offset volumes and difference volumes was done after flattening them on the “Lower Mannville”. This was taken to be the first reflection peak below the coals and is fairly consistent on both components. The Lower Mannville was picked on middle offsets for both components and these picks were used to flatten all volumes.

Considering first the P-P data, Figure 11 shows inline 80 (W-E) on the near, far and far-near difference volumes. In 11A the Lower Mannville is indicated while in 11B an enlargement of the 70ms interval centered on the channel is shown. Also indicated in 11B are four time slices which we judged to be of major interest. The slices at 1138ms

and 1146ms are interpreted to be just above and within the top channel and the final two (1160 and 1162 ms) are within the Glauconite channel. (In all of our gray level displays, black is extreme positive and white is extreme negative.)

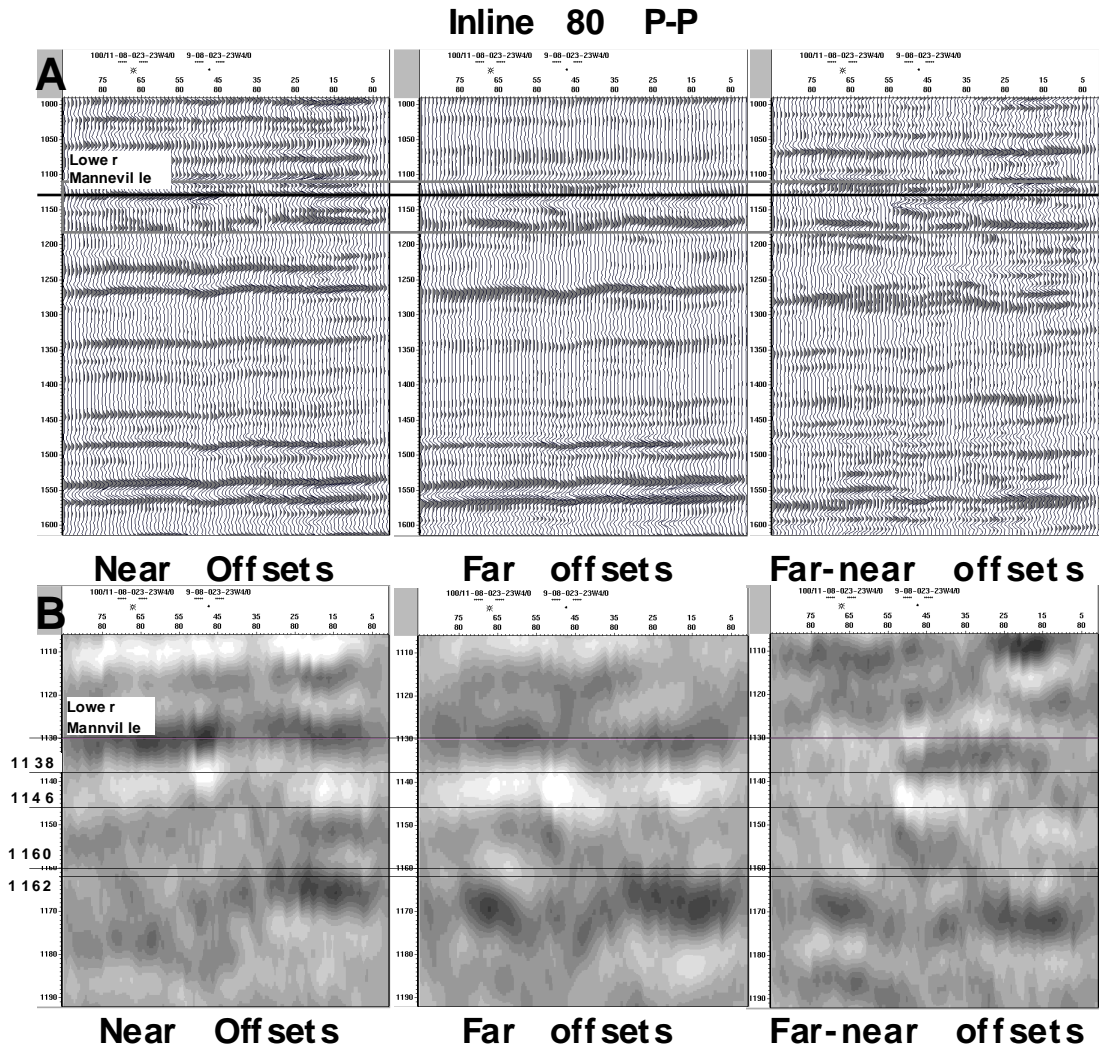


Fig. 11. Inline 80 is shown for the P-P data. A: From the left are the near offset data, the far offset data, and their difference. The data have been flattened on the Lower Mannville which was picked on the middle offset data (not shown). B: An enlargement of the channel portion of A (dashed box).

Figures 12, 13, 14, and 15 are views of the time slices for the four times noted in Figure 11b. For each time slice, the near, far, far-near difference are shown. In all four figures, there are strong AVO anomalies which seem to track (or parallel) the trend of the producing oil wells (white dots).

Figure 12 shows an apparent positive AVO anomaly just above the top channel. We have no ready explanation for this though the strong spatial correlation with the producing wells is intriguing. Both our synthetic seismograms and our Zoeppritz equations analysis fail to predict a strong positive AVO effect associated with the channel top. There are several possible explanations though it seems that the most likely is that the anomaly is a complex interference event caused by NMO tuning at the far offsets. (Our synthetic seismograms did not have NMO effects in them.)

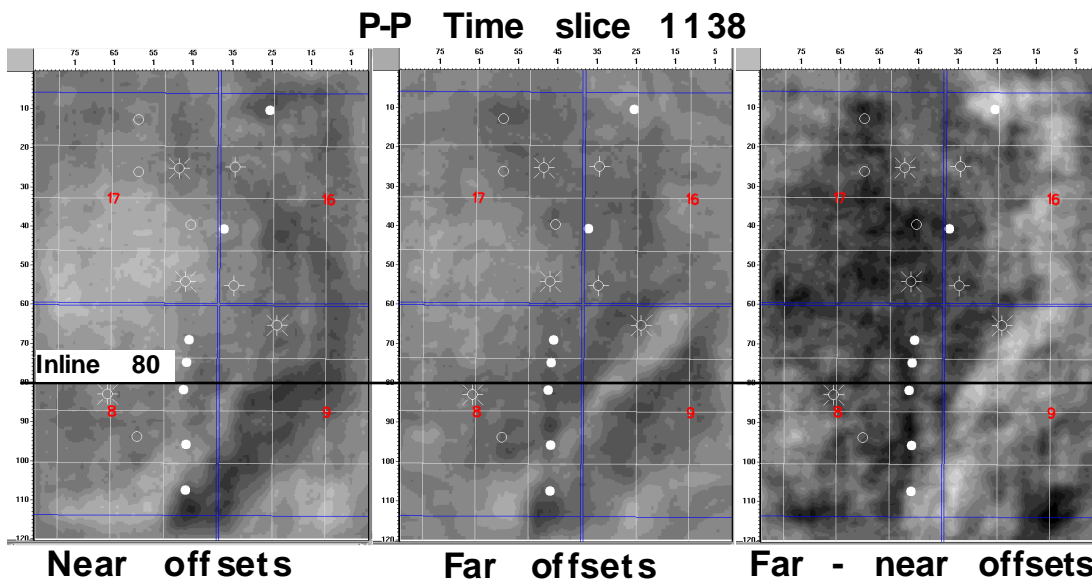


Fig. 12. A time slice through three different P-P volumes at 1138 ms which is interpreted to be just above the top channel. (Figure 11). From left are the near offset volume, the far offset volume, and the Far - near difference volume.

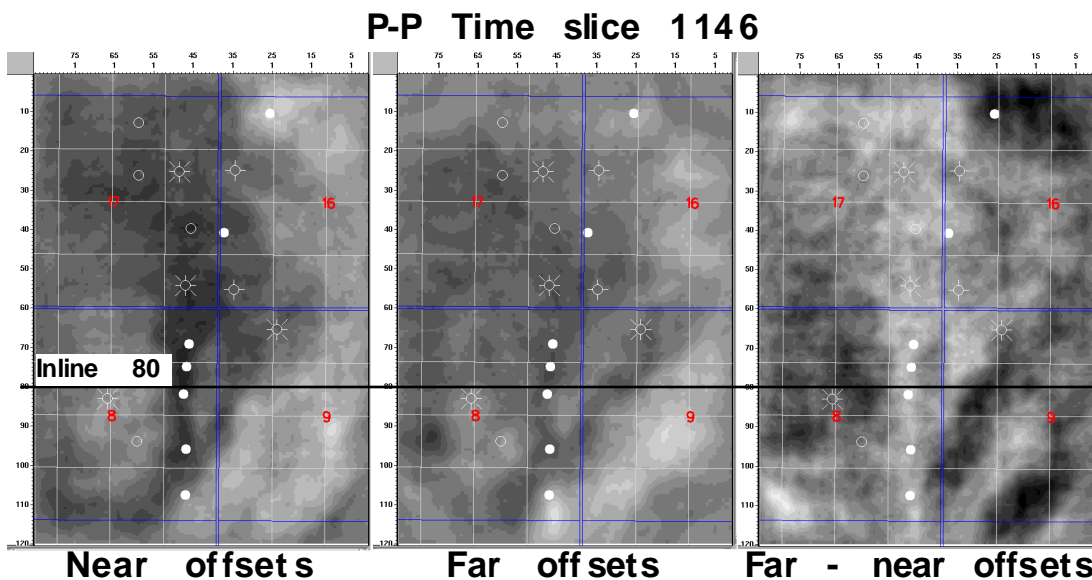


Fig. 13. A time slice through three different P-P volumes at 1146 ms which is interpreted to be within the top channel. (Figure 5). From left are the near offset volume, the far offset volume, and the Far - near difference volume.

Figure 13, which is interpreted as being at the top of the lower channel, is perhaps the most appealing and shows a strong negative AVO anomaly closely tracking the producing wells. This is quite consistent with both the synthetic seismograms and the Zoepritz analysis and is probably a strong indicator of the porous sand channel.

The oil well at the far northeast corner of the survey (13-16) does not seem to be indicated by the AVO anomaly. We note that it is near the survey boundaries and feel that the data processing might not be optimal for such a location.

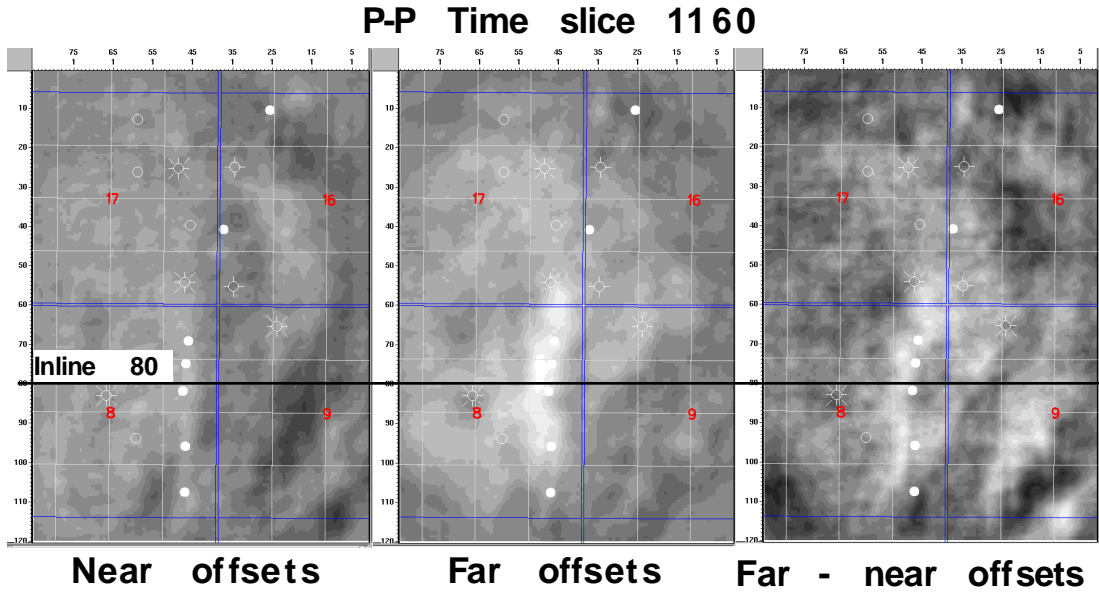


Fig. 14. A time slice through three different P-P volumes at 1160 ms which is interpreted to be within the Glauconite channel. (Figure 5). From left are the near offset volume, the far offset volume, and the Far - near difference volume.

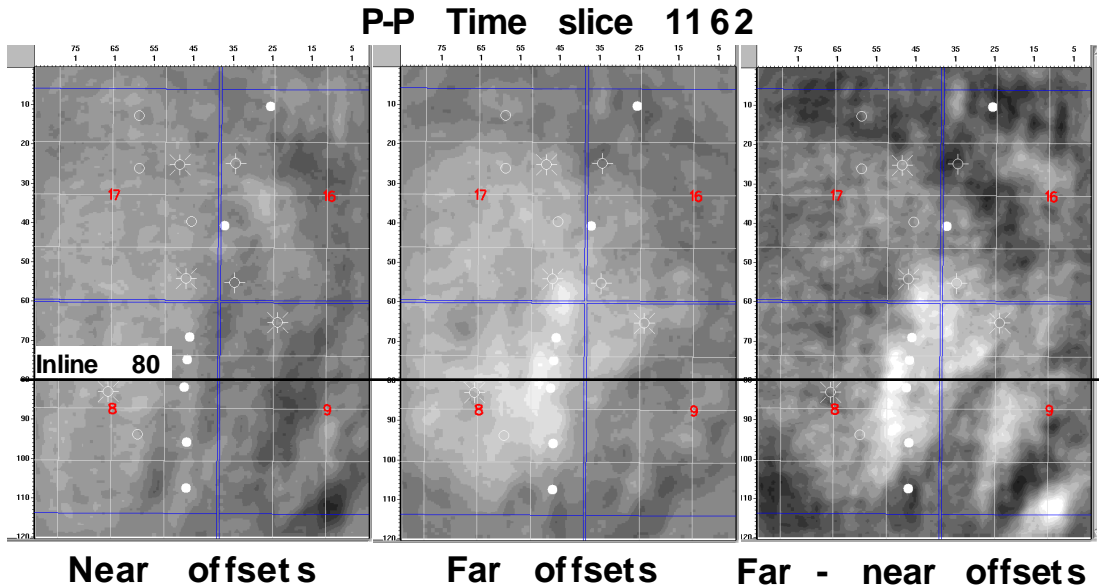


Fig. 15. A time slice through three different P-P volumes at 1162 ms which is interpreted to be within the Glauconite channel. (Figure 5). From left are the near offset volume, the far offset volume, and the Far - near difference volume.

The oil well at the far northeast corner of the survey (13-16) does not seem to be indicated by the AVO anomaly. We have reason to suspect the statics solution for the Sensor processing and the area of greatest concern is the northeast sector of the survey. If the

Figures 14 and 15 show another negative AVO anomaly which we interpret to lie within the Glauconite channel. Though spatially correlated with the well trend, it is displaced 100-200 meters to the west. This suggests that the channel trace has moved eastward from early to later times. It may be that the initial channel anomaly is controlled by structure on the Mississippian unconformity and later channel development moved eastwards in response to a changing environment. This lower channel anomaly, displaced to the west, is also imaged in the converted wave processing of the radial components data (Yang et al., 1996)

Turning now to the P-S data, Figure 16 shows inline 80 (W-E) on the mid, far and far-mid difference volumes. Since the P-S reflections are expected to be vanishingly small at near offsets, the near offset volume was not used (it was very noisy). Examination of figures 5-7 shows that the P-S reflection strength tends to maximize in the middle offsets and decrease on either end. We chose to present mid and far offsets in this report and their difference though, as we shall see, the latter is not a strong diagnostic.

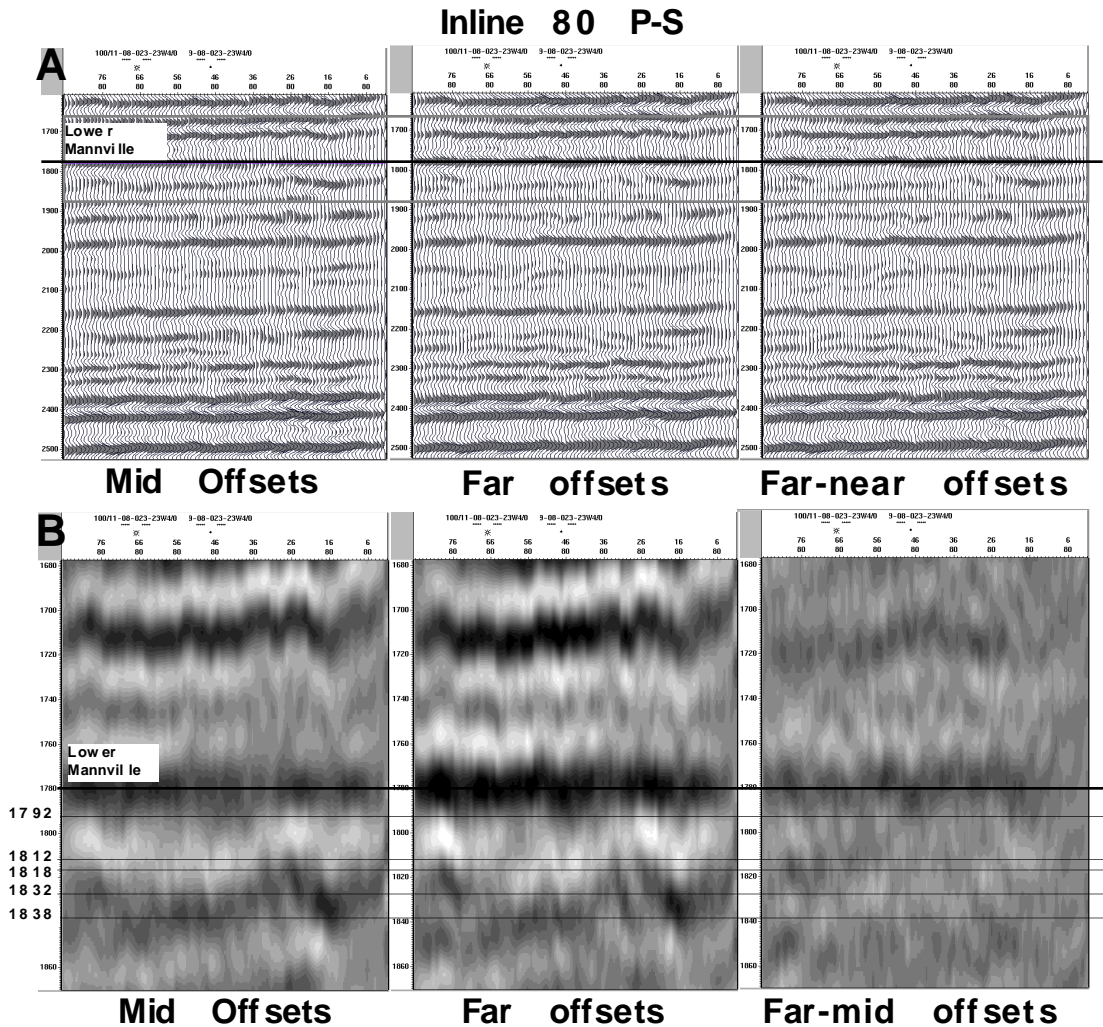


Fig. 16. Inline 80 is shown for the P-S data. A: From the left are the near offset data, the far offset data, and their difference. The data have been flattened on the Lower Mannville which was picked on the middle offset data (not shown). B: An enlargement of the channel portion of A (dashed box).

As with the P-P data, the P-S data was flattened on the Lower Mannville as picked on the mid offset volume. The channel interval is interpreted as extending from roughly 1790 ms to 1840ms in figure 16b. Also shown are the times of the five time slices which we present.

Figures 17, 18, 19, 20, and 21 are five time slices which were felt sufficiently interesting to present here: 1792 ms (above top channel), 1812 and 1818 (within top channel), and 1832 and 1838 (within Glauconite channel).

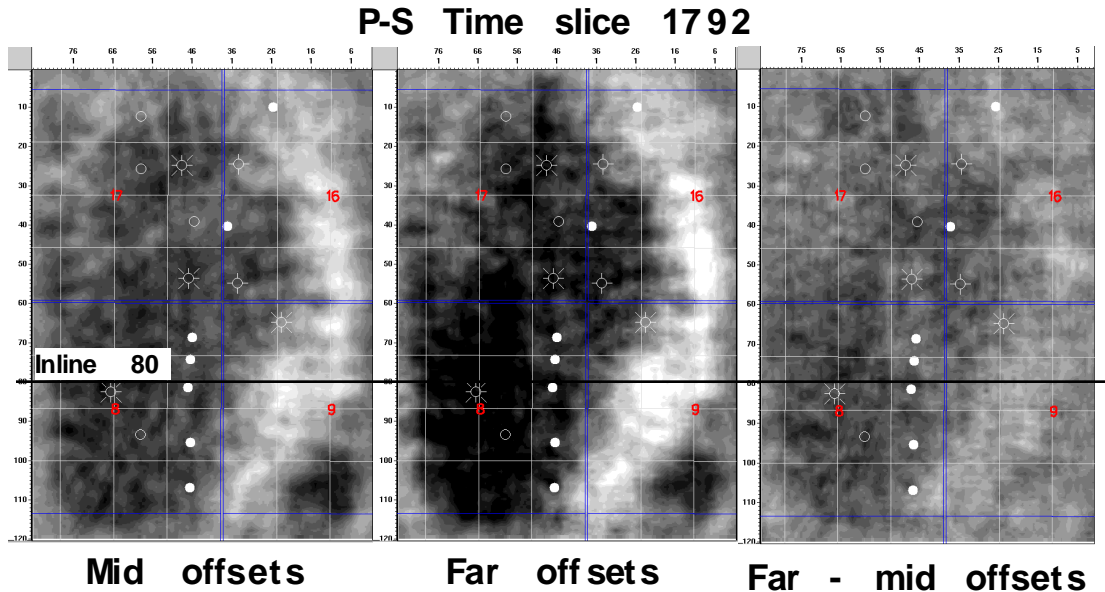


Fig. 17. A time slice through three different P-S volumes at 1792ms which is interpreted to be just above the top channel. From left are the middle offset volume, the far offset volume, and their difference.

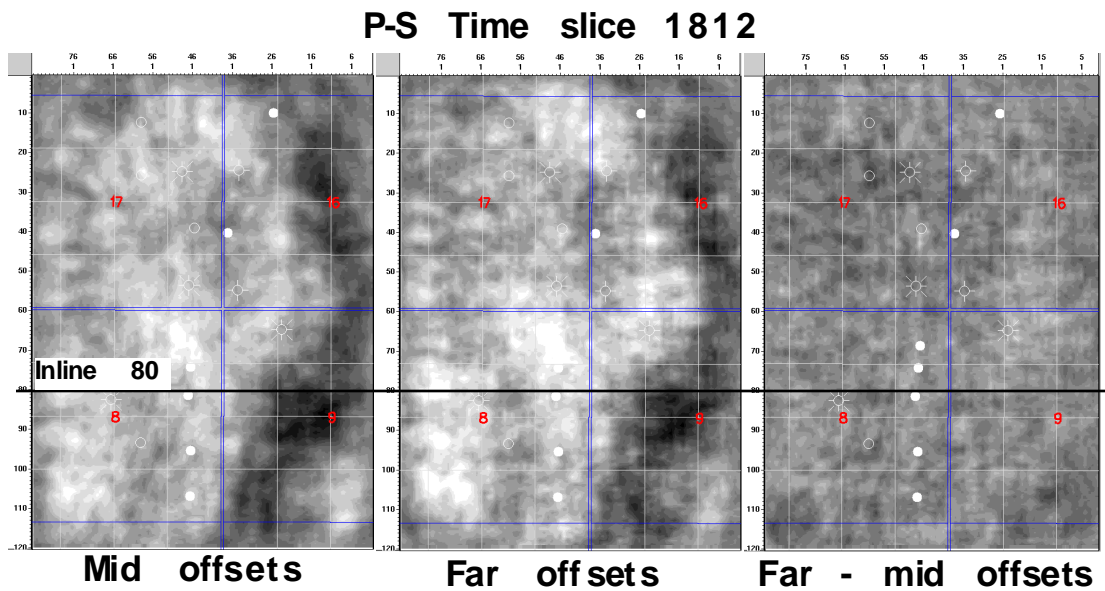


Fig. 18. A time slice through three different P-S volumes at 1812ms which is interpreted to be in the upper part of the top channel. From left are the middle offset volume, the far offset volume, and their difference.

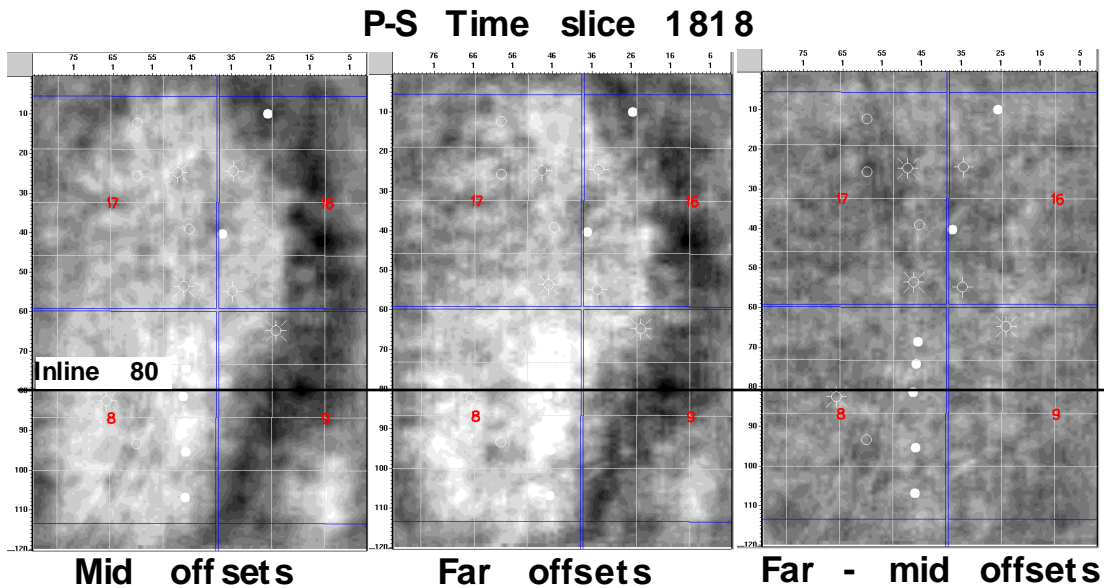


Fig. 19. A time slice through three different P-S volumes at 1818ms which is interpreted to be in the upper part of the top channel. From left are the middle offset volume, the far offset volume, and their difference.

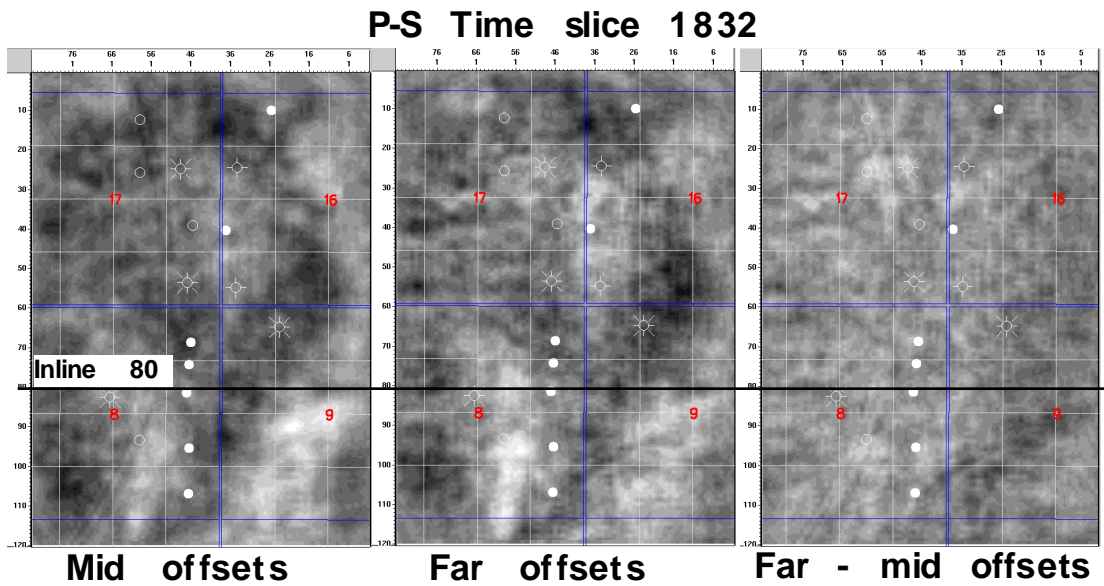


Fig. 20. A time slice through three different P-S volumes at 1832ms which is interpreted to be in the Glauconite channel. From left are the middle offset volume, the far offset volume, and their difference

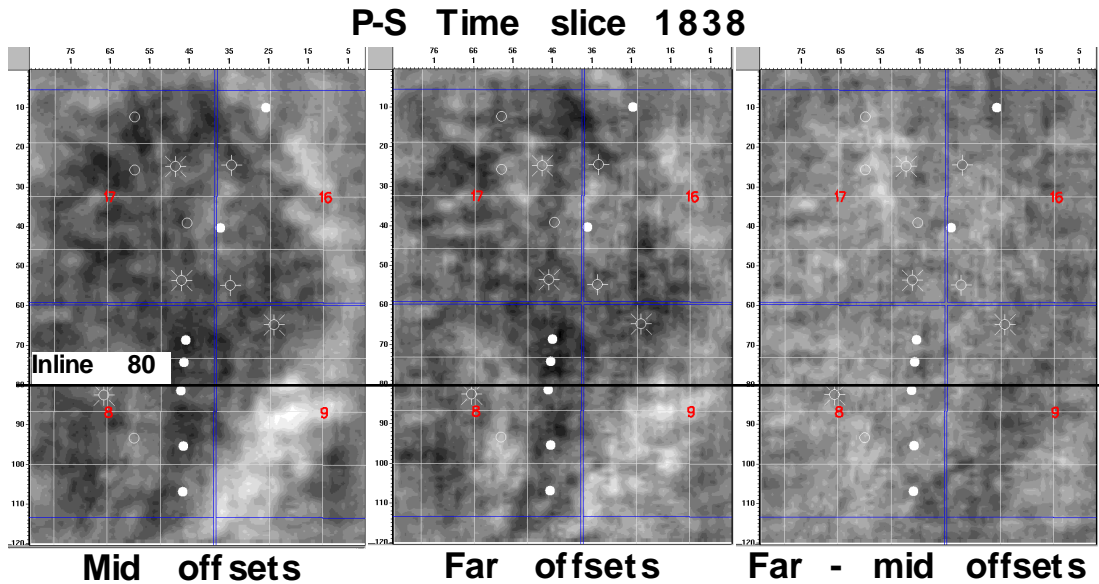


Fig. 21. A time slice through three different P-S volumes at 1832ms which is interpreted to be near the base of the Glauconite channel. From left are the middle offset volume, the far offset volume, and their difference

In assessing these images it should be considered that they were prepared with a P-wave AVO bias. That is, their production was guided by experience with P-waves and, we now realize, that some problems were introduced. Perhaps the most troubling is the loss of relative amplitude information between the different offset volumes due to the fact that they were processed independently. With P-waves, since the dominant behavior is to show very little AVO, it suffices to balance the overall power in each offset volume. On the other hand, with P-S waves, we expect the dominant behavior to be that the far offsets have less power than the middle offsets and so balancing the two volumes is erroneous. In doing so, we have introduced a bias into the apparent AVO. However, we still present our images because they show interesting patterns with intriguing spatial correlations. Roughly speaking, our images show departures from the average behavior such that a negative AVO anomaly, for example, represents amplitude decreasing with offset more strongly than average.

There are several apparent anomalies in the data which seem to correlate with the well trends. For example, in figures 18 and especially 19 a pronounced negative AVO effect can be seen along the trend of producing wells. This correlates quite well with the top channel anomaly which was seen on the P-P data (Figure 13) but seems to be more diffuse. The offset difference volume shows little of interest.

Another interesting anomaly is seen on time slice 1832ms (Figure 20) which shows a trend to the west of the producing wells and again shows strong negative AVO. It seems further west than the image of the Glauconite channel seen in Figures 14 and 15 in the P-P data.

In Figure 21, the far offset volume shows hints of a channel trend extending north from the producing wells though 09-17 (regional) is on this trend. This may well be a feature on the Mississippian which does not directly control channel development.

CONCLUSIONS

There are strong AVO anomalies in the P-P data which seem to indicate both the upper and lower channel sands. These anomalies are, in part, interpretable by simple Zoeppritz equation modeling but also have effects due to tuning and interference with other reflectors. The upper channel trend directly coincides with the producing oil wells in the Blackfoot field while the lower (Glauconite) trend is displaced roughly 100 meters westward. Zoeppritz equation analysis suggests that these anomalies are caused by the strong decrease in Poisson's ratio, from about .32 above the channel to near .21 in the channel as suggested by the 08-08 well. This Poisson's ratio anomaly is not seen in non-oil wells including 12-16 which penetrated shale plugged channel.

There are also intriguing anomalies in the P-S AVO images which also have some correlation with well control but are not as definitive as those seen with the P-P data. The processing flow used to create the images was designed with P-P reflections in mind and was not optimal for converted wave data.

It is our intent to follow this work with a more detailed analysis, including examination of the Pulsonic data and possible reprocessing of the entire volume.

ACKNOWLEDGMENTS

We thank the Sponsors of the Blackfoot 3C-3D group shoot and the Sponsors of the CREWES Project for their financial support. We also thank Don Lawton for helpful suggestions.

REFERENCES

- Aki, K. T., and Richards, P.G., 1980, Quantitative Seismology: Theory and Methods, Vol. 1., W.H. Freeman.
- Lawton, D. C., and Howell, T. C., 1992, P-P and P-SV synthetic stacks, Expanded Abstract, 62nd SEG Annual International Meeting, October 25-29, New Orleans, USA, 1344-1347
- Margrave, G. F., and Foltinek, D. S., 1995, Synthetic P-P and P-SV cross sections, CREWES Annual Research Report, Vol. 7.
- Ross, C. P., and Beale, P. L., 1994, Seismic offset balancing: Geophysics, 59, 93-101
- Schoepp, A. R., and Margrave, G. F., 1996, Signal band measurements on the Blackfoot 3C-3D with comparison to the Blackfoot Broadband experiment: CREWES Annual Research Report, Vol. 8
- Simmons, J. L., and Backus, M. M., 1994, AVO modeling and the locally converted shear wave: Geophysics, 59, 1237-1248
- Smith, G. C., and Gidlow, P. M., 1987, Weighted stacking for rock property estimation and detection of gas: Geophysical Prospecting, 35, 993-1014
- Simin, V., Harrison, M. P., and Lorentz, G. A., 1996, Processing the Blackfoot 3C-3D seismic survey: CREWES Annual Research Report, Vol. 8
- Stewart, R., Ferguson, R., Miller, S., Gallant, E., and Margrave, G, 1996, The Blackfoot Seismic Experiments: Broad-band, 3C-3D, and 3D VSP surveys, CSEG Recorder (June 1996)
- Yang, G. Y. C., Lawton, D. C., Stewart, R. R., Miller, S. L. M., Potter, C. C., and Simin, V., 1996, Interpretation and analysis of the Blackfoot 3C-3D seismic survey: CREWES Annual Research Report, Vol. 8